



## Changes in $\nu g_{9/2}$ shape polarisation across the odd neutron-rich Cr isotopes

A.N. Deacon<sup>a</sup>, S.J. Freeman<sup>a</sup>, R.V.F. Janssens<sup>b</sup>, F.R. Xu<sup>c</sup>, M.P. Carpenter<sup>b</sup>,  
I.R. Calderin<sup>d</sup>, P. Chowdhury<sup>e</sup>, N.J. Hammond<sup>b</sup>, T. Lauritsen<sup>b</sup>, C.J. Lister<sup>b</sup>,  
D. Seweryniak<sup>b</sup>, J.F. Smith<sup>a</sup>, S.L. Tabor<sup>d</sup>, B.J. Varley<sup>a</sup>, S. Zhu<sup>b</sup>

<sup>a</sup> *Schuster Laboratory, University of Manchester, Manchester M13 9PL, UK*

<sup>b</sup> *Argonne National Laboratory, Argonne, IL 60439, USA*

<sup>c</sup> *Department of Technical Physics, Peking University, Beijing 100871, China*

<sup>d</sup> *Department of Physics, Florida State University, Tallahassee, FL 32306, USA*

<sup>e</sup> *University of Massachusetts, Lowell, MA 01854, USA*

Received 30 March 2005; received in revised form 4 June 2005; accepted 4 July 2005

Available online 13 July 2005

Editor: V. Metag

### Abstract

Excited states in  $^{57}\text{Cr}$  have been populated to high spin in the  $^{14}\text{C}(^{48}\text{Ca}, \alpha n)$  reaction at a beam energy of 130 MeV. A regular sequence of stretched quadrupole transitions has been established above the yrast  $9/2^+$  level. This sequence is interpreted as a rotational band associated with prolate deformation induced by the excitation of the odd neutron into the  $1/2^+[440]$  orbital. Total Routhian surface calculations, which follow this configuration to high spin, reproduce the observed features of the band. They are also able to account for a similar, but less well developed structure in  $^{55}\text{Cr}$ . In contrast, the isomeric yrast  $9/2^+$  state in  $^{59}\text{Cr}$  appears to be a band-head state dominated by the  $9/2^+[404]$  configuration, which is favoured at oblate deformations. Such a marked difference presents a significant challenge for theoretical descriptions, but is consistent with features exhibited by the low-lying negative-parity states in  $^{59}\text{Cr}$ .

© 2005 Elsevier B.V. All rights reserved.

PACS: 23.20.Lv; 27.40.+z; 27.50.+e

Considerable effort is currently focused on developing a proper understanding of the structure of

neutron-rich nuclei. The basic motivation for such studies is the mounting evidence that these nuclei reveal aspects of the nuclear force that are not readily apparent in stable and neutron-deficient systems. Applying the nuclear shell model, one of the corner stones of our present understanding, to neutron-rich nuclei

*E-mail address:* [sean.freeman@manchester.ac.uk](mailto:sean.freeman@manchester.ac.uk)  
(S.J. Freeman).

requires the development of novel effective interactions within new model spaces. Recent efforts to apply the full  $\pi f_{7/2} \nu fp$  space to neutron-rich nuclei above doubly-magic  $^{48}\text{Ca}$  typify such an approach [1]. In this particular case, the role of a strong proton–neutron ( $\pi$ – $\nu$ ) monopole interaction has been highlighted as it causes significant shifts in the energy of the  $\nu f_{5/2}$  state as the  $\pi f_{7/2}$  orbital fills. In fact, the monopole shift, combined with a relatively low single-particle level density, conspires to produce an unexpected  $N = 32$  subshell closure in Ca, Ti and Cr nuclei [2–5].

The success of calculations employing the fp model space depends sensitively on the size of the  $N = 40$  subshell gap. A large gap effectively isolates the low-lying structure from the  $\nu g_{9/2}$  orbital and would bode well for the efficacy of the fp space. On the other hand, a weak subshell closure facilitates single-particle excitations outside the model space, leading to difficulties with calculations that ignore the  $\nu g_{9/2}$  level, as appears to be the case for nuclei with  $N \geq 35$  [6]. Neutron excitations into the  $g_{9/2}$  state should have clear structural consequences as this orbital has considerable potential for polarising the nuclear shape via strong deformation-driving effects. The chromium isotopes lie in the middle of the  $\pi f_{7/2}$  shell and would, therefore, be expected to display some of the strongest collective effects. In fact, contrary to previous claims of large stable ground-state deformation [7], recent studies of the detailed structure of even–even Cr isotopes indicate considerable softness in shape [8,9] and the degree of softness appears to increase with neutron number. With such pliant cores, odd Cr isotopes are expected to show considerable polarisation in shape when valence particles are excited into eccentric orbits such as the  $\nu g_{9/2}$  single-particle state.

This Letter reports the first in-beam study of excited states in  $^{57}\text{Cr}$  and extends the previously known level scheme, deduced from  $\beta$  decay [10], to considerably higher spin. It establishes experimental evidence for prolate polarisation with the excitation of a  $g_{9/2}$  neutron and an adequate theoretical description is found using total Routhian surface (TRS) calculations. The success of the calculations extends to a similar, but less well delineated band structure in  $^{55}\text{Cr}$  [11]. Surprisingly, this is in contrast to the situation in  $^{59}\text{Cr}$ , the most neutron-rich isotope for which excited states are known [6]. In this case there is evidence for *oblate* rather than prolate polarisation. This abrupt change in

the type of polarisation outside a soft core presents a challenge for theoretical descriptions, but appears consistent with features of the low-lying negative-parity states in  $^{59}\text{Cr}$ .

The techniques employed in the production and identification of events corresponding to  $^{57}\text{Cr}$  were similar to those used in a previous study of  $^{59}\text{Cr}$  [6] where more details can be found. A  $^{48}\text{Ca}$  beam, accelerated to 130 MeV using the ATLAS accelerator at Argonne National Laboratory, was used to bombard a  $100\text{-}\mu\text{g cm}^{-2}$  thick  $^{14}\text{C}$  target, enriched to approximately 90% with  $^{12}\text{C}$  as the main contaminant. Prompt  $\gamma$  rays were detected with the gamma-sphere array [12] which consisted of 100 Compton-suppressed germanium detectors. Recoiling reaction products were separated from beam particles and dispersed according to their mass-to-charge ( $A/q$ ) ratio with the Fragment Mass Analyzer (FMA) [13]. The FMA was adjusted to transport ions with mass 60 and charge state  $17^+$  to the centre of the focal plane, but those with  $A/q = 57/16$  also fell within the spectrometer acceptance. A parallel-grid avalanche counter located at the focal plane enabled the position of the ions to be measured and timing signals to be generated. A segmented ion chamber recorded the energy-loss characteristics of the recoils behind the focal plane. The data acquisition was triggered by the arrival of an ion at the focal plane in coincidence with the detection of at least one prompt  $\gamma$  ray.

The time-of-flight through the spectrometer system,  $T$ , was combined with the total energy,  $E$ , to produce the parameter  $ET^2$  which is proportional to the mass of the ion. In a two-dimensional plot of  $ET^2$  versus  $A/q$ , ions with  $A = 57$  and  $q = 16$  are clearly separated from other events as illustrated in Fig. 1(a). Although  $A = 57$  ions are the most prolifically produced of those detected at the focal plane, a polygonal gate on this group effectively removes contaminating channels corresponding to  $^{60}\text{Fe}$  and  $^{56}\text{Cr}$ . A spectrum of energy loss,  $\Delta E$ , against total energy,  $E$  [Fig. 1(b)], demonstrates that unit- $Z$  separation was achieved. The Cr ions involve the evaporation of  $\alpha$  particles and they form two distinct groups in this spectrum, in contrast to ions from other reaction channels which appear as stripes. The two groups correspond to  $\alpha$  emission in directions parallel and antiparallel to that of the beam, resulting in a significant momentum boost to the recoils. When evap-

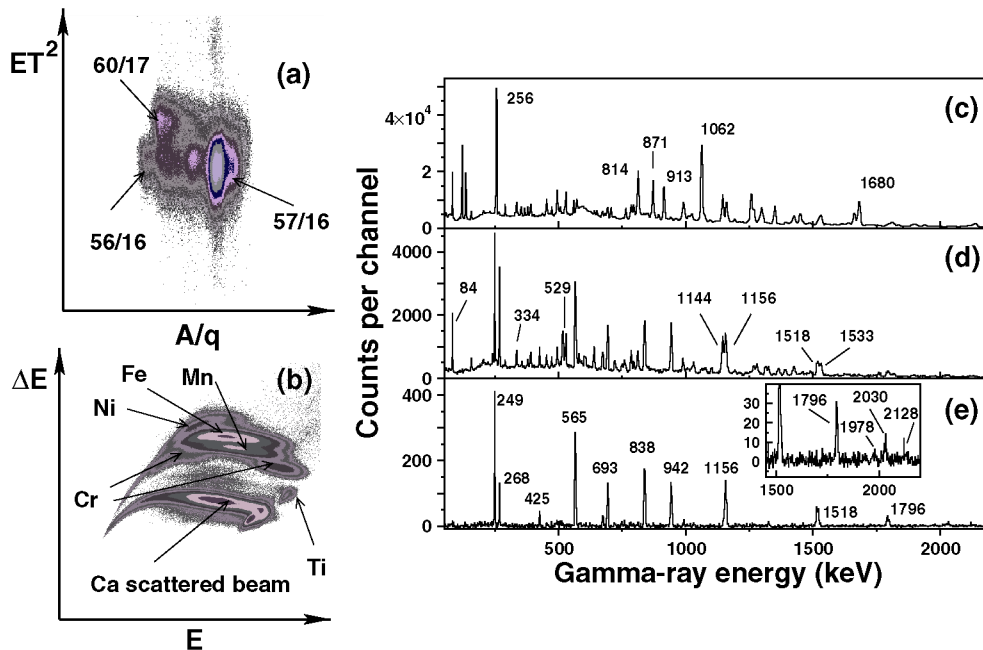


Fig. 1. (a) A two-dimensional spectrum of charge-to-mass ratio,  $A/q$ , against  $ET^2$ , as defined in the text. Various ion groups in this spectrum are labelled by their  $A/q$  ratios. (b) A two-dimensional spectrum of the energy-loss signal,  $\Delta E$ , against the total energy,  $E$ , for ions entering the ionisation chamber. (c) A prompt  $\gamma$ -ray energy spectrum for ions with  $A = 57$  and  $q = 16$ . (d) A  $\gamma$ -ray spectrum for ions with  $Z = 24$ ,  $A = 57$  and  $q = 16$ . (e) A coincident  $\gamma$ -ray spectrum with the same conditions as (d), but additionally requiring the observation of a  $\gamma$  ray with energies of 565, 838, 1156 or 1796 keV. Peaks in the spectra (c)–(e) are labelled by their transition energy to the nearest keV, see text for details.

oration occurs perpendicular to the beam direction the induced momentum boost effectively removes the recoils from the FMA acceptance. Also shown are prompt  $\gamma$ -ray spectra for events passing certain conditions. Fig. 1(c) provides the spectrum in coincidence with  $A = 57$  ions. This is dominated by transitions in  $^{57}\text{Fe}$  with, for example, energies of 256, 814, 871, 913, 1062 and 1681 keV assigned from previous work [14]. Placing an additional condition on ions with  $Z = 24$  [Fig. 1(d)] effectively suppresses these lines, although there is some minor leakthrough from  $^{57}\text{Mn}$  [15], such as the 84-, 529-, 1145- and 1534-keV transitions. The energies of transitions identified in  $^{57}\text{Cr}$  are listed in Table 1. Further evidence for the mutual association of the candidate  $^{57}\text{Cr}$  transitions can be obtained through an analysis of  $\gamma\gamma$  coincidence relationships. As an example of the quality of the coincidence spectra, Fig. 1(e) presents a  $A/q = 57/16$ ,  $Z = 24$   $\gamma$ -ray spectrum additionally gated on the observation of transitions within the regular high-spin band in  $^{57}\text{Cr}$ ,

discussed below, with energies of 565, 838, 1156 or 1796 keV.

The deduced level scheme is presented in Fig. 2. The transitions between levels up to an excitation energy of 942 keV are in agreement with the previous level scheme deduced from  $\gamma\gamma$  events following the  $\beta$  decay of  $^{57}\text{V}$  [10]. No spin assignments were proposed in that work. Ref. [10] also observed transitions with energies of 1314.3 and 892.5 keV de-exciting a 1581-keV excited state; here, evidence is found only for the former. The spin assignments given in Fig. 2 were made on the basis of the measured angular distributions, combined with a ground-state spin of  $3/2^-$  deduced from the measured  $\beta$ -decay feeding pattern to  $^{57}\text{Mn}$  [16]. Fits to the angular distributions used the form  $W(\theta) = A_0[1 + a_2P_2(\cos\theta)]$  as it was difficult to extract statistically significant  $a_4$  terms. The extracted  $a_2$  coefficients are listed in Table 1 and were used to identify stretched dipole and quadrupole transitions. The

Table 1

Energies and spins of excited states in  $^{57}\text{Cr}$ . Measured transition energies, relative intensities (corrected for efficiency and internal conversion) and the angular distribution coefficients,  $a_2$ , of de-exciting  $\gamma$  rays are listed. The  $a_2$  coefficients marked with an asterisk are derived from the angular distribution of the total area of an unresolved doublet

Level energy (keV)	$J^\pi$	Transition energy (keV)	Relative intensity	$a_2$
267.87(11)	$5/2^-$	267.92(9)	65.7(24)	-0.09(5)
692.69(13)	$5/2^-$	424.90(14)	14.8(10)	
		692.61(12)	60(3)	-0.44(8)
941.79(15)	$7/2^-$	249.08(8)	60.9(22)	-0.16(5)
		673.8(2)	28.3(18)	
		941.75(18)	100(5)	+1.1(1)
1506.9(2)	$9/2^{(+)}$	565.11(10)	89(5)	-0.30(4)
1581.1(3)	$9/2^{(-)}$	639.1(2)	29.5(17)	-0.31(8)
		1313.8(4)	8.3(24)	+0.19(9)
1857.9(5)	$(9/2^-)$	1166.5(6)	6.4(13)	
		1593.8(17)	10.5(24)	
2098.2(3)	$11/2^{(-)}$	240.8(4)	4.6(6)	
		516.88(19)	33.3(20)	
		1156.0(4)	49(12)	+0.19(4)*
2344.5(3)	$13/2^{(+)}$	837.59(12)	88(5)	+0.18(5)
2611.6(4)	$(13/2^-)$	513.4(2)	15.2(16)	
		1030.8(5)	20(10)	
3377.6(8)		1279.4(5)	33(3)	
3500.4(4)	$17/2^{(+)}$	1155.9(2)	69(7)	+0.19(4)*
3555.4(7)	$(15/2^-)$	943.8(4)	22(3)	-0.77(7)
4136.4(11)		758.8(5)	13.5(18)	
4827.1(21)		1326.6(14)	19.0(25)	
4856.3(17)		720.0(8)	12.9(13)	
4920.1(14)		1364.7(8)	16.0(25)	
5018.7(7)	$21/2^{(+)}$	1518.2(4)	57(3)	+0.20(11)
6814.7(14)	$(25/2^+)$	1796.0(8)	27.7(22)	
8844(3)	$(29/2^+)$	2029.7(18)	16(3)	
10972(7)	$(33/2^+)$	2128(4)	8.6(19)	
12950(9)	$(37/2^+)$	1978(4)	6.5(17)	

presence of many cross-over transitions in the level scheme gives further confidence to some of these assignments.

The observed scheme divides naturally into two groups of states. Firstly, a sequence of rather irregular levels is based on the ground state. Negative parity is assigned to at least the lowest lying levels on the basis of their population in  $\beta$  decay [10]. These states are based on excitations of fp-shell neutrons; there is general agreement between the observed levels and those calculated by the spherical shell model with a full fp-shell basis and the GXPF1A interaction (not shown here) [17,18]. Secondly, there is a group of levels which form a regular band composed of stretched quadrupole transitions based on a spin-9/2 state at 1507 keV. This band is assigned positive parity; a sim-

ilar structure exists in  $^{55}\text{Cr}$ , where linear polarisation measurements were performed [11]. The present results complete the systematic picture of the yrast  $9/2^+$  states in odd-Cr nuclei from  $N = 29$  to 35; it is the interpretation of these states that is discussed below.

In the  $^{52}\text{Cr}(d, p)^{53}\text{Cr}$  reaction,  $\ell = 4$  transfer strength is seen at 3.715 MeV with a significant spectroscopic factor [19]. Given the proximity to  $N = 28$ , it is likely that this corresponds to near-spherical  $g_{9/2}$  strength. In  $^{55,57}\text{Cr}$ ,  $9/2^+$  states are seen at excitation energies of 2.870 and 1.507 MeV, respectively, and a regular sequence of E2 transitions is observed above these states in both cases. Given recent observations which show that the shape of even-even Cr nuclei becomes progressively softer with neutron number [8, 9], an interpretation of the regular sequences as be-

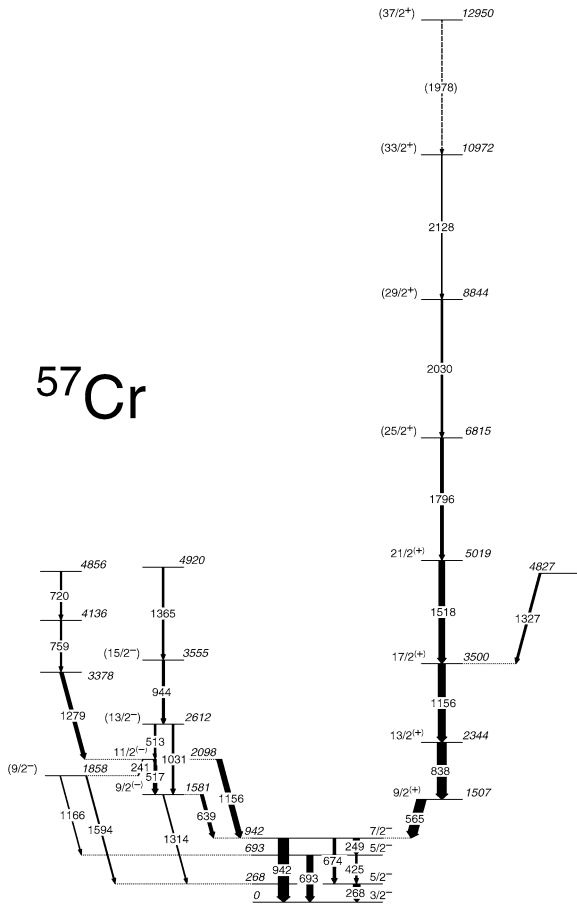


Fig. 2. The level scheme for  $^{57}\text{Cr}$  deduced in the present work. The levels are labelled by their spin-parity and excitation energy. The widths of the arrows indicate the relative intensity of the  $\gamma$ -ray transitions, normalised to ground-state feeding.

ing associated with deformed rotational bands arising from the polarisation of the even–even core by an odd neutron is suggested. In the case of  $^{57}\text{Cr}$ , the observed spins are too high to be accommodated by excitations within a simple fp model space and require excitations involving the  $\nu g_{9/2}$  single-particle state. In fact, the highest observed spin, tentatively  $37/2$ , is equal to the maximum value expected for a  $\pi f_{7/2}^4 \nu g_{9/2} (f_{5/2} p_{3/2} p_{1/2})^4$  valence configuration.

The observed band is most likely decoupled in nature as it is composed of only one of the two signature partners. This observation in turn suggests a configuration based on the lowest  $\Omega = 1/2^+$  orbital, arising from  $g_{9/2}$  spherical parentage, which is favoured in

the presence of prolate deformation. The decoupling parameter for the  $1/2^+[440]$  Nilsson orbital is large,  $a \sim 5.0$  [20]. The combination of this value with a rotational parameter estimated from the excitation energies of the lower spin members of the band results in the prediction that the  $3/2^+$  member of the unfavoured sequence lies at an excitation energy comparable to that of the  $13/2^+$  member of the favoured sequence. This is sufficiently non-yrast to be unobserved in heavy-ion fusion evaporation reactions. Note that in a similar fashion, the  $1/2^+$  and  $5/2^+$  band members are estimated to lie  $\sim 120$  and  $\sim 360$  keV below the  $9/2^+$  state, but these states are not seen in the current data. Using typical transition rates ( $10^{-3}$  to  $10^{-4}$  w.u. for E1 transitions and 10 W.u. for E2 transitions [21]), the branching ratio of a 360-keV in-band  $9/2^+ \rightarrow 5/2^+$  E2 transition, not seen here, to the observed 565-keV E1 out-of-band transition was estimated to be in the range 0.4–4%. The experimental upper limit that can be placed on the intensity of a currently unobserved transition in the range 250 to 500 keV is 3–4% of the intensity of the 565-keV transition. The in-band  $9/2^+ \rightarrow 5/2^+$  transition is therefore probably too weak to be apparent in these data. The  $1/2^+$  bandhead state would be fed by an E4 transition from the  $9/2^+$  state. These considerations are consistent with the non-observation of the  $1/2^+$  and  $5/2^+$  band members in the current data.

Total Routhian surface (TRS) calculations for  $^{57}\text{Cr}$  were performed. The diabatic blocking procedures discussed in Ref. [22] were followed to track, as a function of rotational frequency, the  $\Omega^\pi = 1/2^+$  intrinsic state corresponding to the  $1/2^+[440]$  Nilsson orbital at zero  $\gamma$  deformation. The Woods–Saxon single-particle parameters used were the so-called “Universal” set from Ref. [23]. The results are shown in Fig. 3, where at low rotational frequency [see Fig. 3(a)] a deep prolate minimum appears with deformation parameters  $\beta_2 = 0.22$  and  $\gamma \sim 0^\circ$ . With increasing rotational frequency, the nucleus remains approximately axially symmetric, but the magnitude of the quadrupole deformation decreases somewhat [Fig. 3(b) and (c)]. The calculations also reproduce experimental observables such as the excitation energies and the single-particle alignments. The left-hand panel of Fig. 3 illustrates the comparison of the experimental aligned angular momentum,  $I_x$ , with that predicted from the TRS calculations; the upbend in

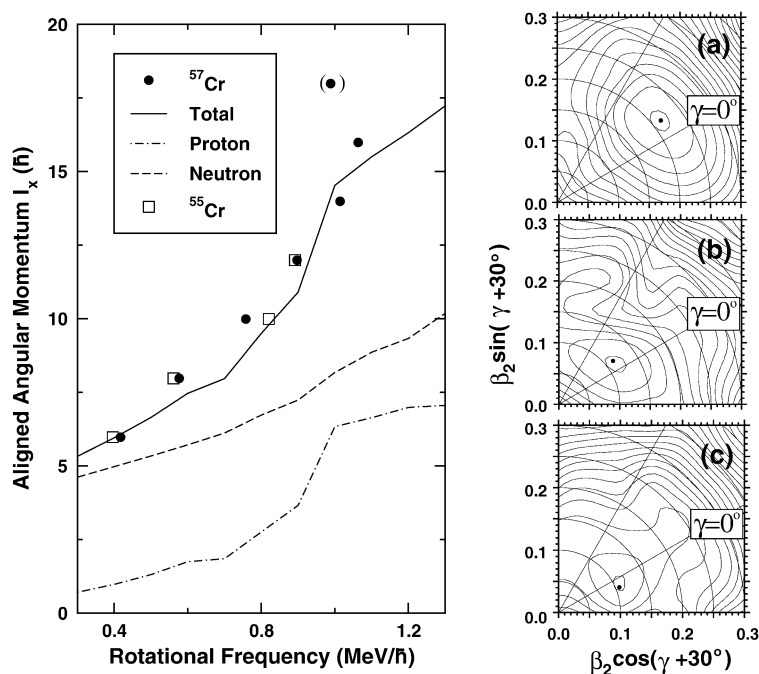


Fig. 3. The results of tracked TRS calculations for the lowest  $\Omega = 1/2^+$  configuration in  $^{57}\text{Cr}$ . The potential energy surfaces are shown for rotational frequencies of (a) 0.2 MeV/ $\hbar$ , (b) 0.9 MeV/ $\hbar$  and (c) 1.4 MeV/ $\hbar$ . Contours are shown at 200 keV intervals and a dot is used to show the location of the absolute minimum. The left-hand portion of this figure presents the experimental angular momentum aligned along the rotation axis,  $I_x$ , as a function of rotational frequency. The point in parentheses is derived from the highest level populated which is tentative in nature. The dashed and dashed-dotted lines represent the contributions from neutrons and protons, shown separately, and the solid line is the total calculated alignment. The experimental alignment in the analogous band in  $^{55}\text{Cr}$  is also given [11].

the data towards the highest spins originates from a  $\pi f_{7/2}^2$  alignment. Such alignment is also responsible for the reduction in deformation noted above. TRS calculations also reproduce the properties of the analogous band in  $^{55}\text{Cr}$  [11], although the sequence in this nucleus is not established experimentally to as high angular momentum as the band in the current data. Nevertheless, the comparison of the aligned angular momentum given in Fig. 3 further indicates the similarity between them. A clear and consistent picture of prolate deformation in the yrast  $9/2^+$  states in  $^{55,57}\text{Cr}$  therefore emerges from the rotational character of the sequence of states based on them, the decoupled nature of the bands and the reproduction of their rotational behaviour with TRS calculations.

A cursory glance at the structure of  $^{59}\text{Cr}$  [6,24] might suggest a similar interpretation: the low-lying levels are irregular and of negative parity, and a  $9/2^+$  state is present at low excitation energy (503 keV), just

as in  $^{55,57}\text{Cr}$ . However, there are some abrupt and surprising changes in behaviour. First, the spherical shell-model calculations which were generally successful in  $^{55,57}\text{Cr}$ , fail to reproduce the low-lying negative-parity states in  $^{59}\text{Cr}$  [18] and the sequence of spins is consistent with a small oblate deformation [6]. In addition, the yrast  $9/2^+$  state is *isomeric* in  $^{59}\text{Cr}$  with a half life of 96(20)  $\mu\text{s}$  [24], and this presents problems if the structure is to be interpreted in an analogous way to  $^{55,57}\text{Cr}$ . Whilst there is significant decoupling for a band based upon the  $1/2^+[440]$  intrinsic state, the  $1/2^+$  and  $5/2^+$  rotational band members would still lie at energies below the  $9/2^+$  state, as discussed above. It is, therefore, difficult to reconcile the extent of the isomerism with this assignment, given the availability of in-band de-excitation paths. The structure of the yrast  $9/2^+$  state in  $^{59}\text{Cr}$  clearly differs from that in  $^{55,57}\text{Cr}$ . The  $\mu\text{s}$  half-life of this state suggests that it is an intrinsic state with no available in-band de-

cay paths; the de-excitation with lowest multipolarity is then via an M2 transition to the yrast  $5/2^-$  state, accounting for the observed isomerism [6,24].

Experimental estimates of the spherical  $N = 40$  subshell gap yield an energy of the order of 2–3 MeV. For example, the average excitation energy, weighted by spectroscopic strength, of the  $\ell = 1$  transfer in the  $^{52}\text{Cr}(d, p)$  reaction is 1.4 MeV. This is to be compared to 3.7 MeV for  $\ell = 4$  strength [19]. Similar energies are used in theoretical approaches; as an example, a gap of 3.4 MeV between  $\nu 2p_{1/2}$  and  $\nu 1g_{9/2}$  levels has been used in shell-model calculations of  $^{56-78}\text{Ni}$  [25]. The appearance of a  $9/2^+$  state at only 0.503 MeV in  $^{59}\text{Cr}$ , significantly less than the size of the spherical  $N = 40$  gap, therefore requires attention. Whilst unlikely, such a large reduction in the energy of states based upon the  $\nu g_{9/2}$  orbital in spherical neutron-rich systems cannot be completely ruled out from the data available at present: the shell-model calculations that would be needed to assess fully the applicability of such an interpretation would involve the extended fp<sub>g</sub> space and these are currently unavailable. An alternative explanation, consistent with the increasingly soft nuclear core, would be the polarisation of an *oblate* shape, lowering the  $\Omega = 9/2^+$  intrinsic state arising from  $\nu g_{9/2}$  parentage. Such an oblate structure, dominated by the  $9/2^+[404]$  Nilsson configuration, would be consistent with the observed excitation energy and isomerism. In fact, as shown in Ref. [6], the sequence of yrast negative-parity states is consistent with a modest oblate deformation, suggesting that the core already has some tendency towards oblate shapes and the excitation of a  $g_{9/2}$  neutron would then drive it further in this direction. An additional experimental indicator would consist of the observation of a coupled band built on the  $9/2^+$  state, but current experimental techniques have unfortunately only yielded a single transition feeding the isomer [6].

To investigate further the possibility of an oblate shape, TRS calculations were carried out. It was not necessary to track specific configurations in this case, at least for low rotational frequencies. Although the actual configuration changes across the calculated potential energy surface in an untracked calculation, near the oblate axis, the  $9/2^+[404]$  Nilsson level always lies lowest. The surfaces arising from such calculations for yrast positive-parity configurations in  $^{55-59}\text{Cr}$

all have a flat shoulder reaching the oblate axis. There is increasing softness in shape with neutron number, particularly in the triaxial direction. For  $^{59}\text{Cr}$ , the potential energy surface near the oblate axis is very flat around  $\beta_2 \sim 0.2$ , but no real minimum appears and the overall surface is very  $\gamma$  soft. The calculations were repeated with several other parameter sets available in the literature [23,26]. The detailed results from calculations with these different parameters depend on the set used, but each gives a similar, very soft and flat potential landscape. In such a scenario, the equilibrium shape is very sensitive to small inadequacies in the calculations, such as couplings between the oblate configuration and the soft core, which are not taken into account. Therefore, it may not be surprising that the comparison of TRS calculations with the experimental deductions is not more favourable in  $^{59}\text{Cr}$ . It must also be remembered that each of these parameter sets was deduced in other mass regions, nearer stability or for neutron-deficient nuclei. Some attention, therefore, needs to be paid to the question of appropriate parameters for this neutron-rich region. Admittedly, there is probably insufficient experimental data at the present time to carry out a proper optimisation and further investigations are needed.

The abrupt changes in structure across the neutron-rich Cr isotopes appear as a result of low single-particle level density which leads to energy gaps in the level structure at both oblate and prolate deformation. Similar phenomena are seen in  $N = Z$  nuclei with  $A \sim 60-70$ , where protons *and* neutrons fill the same orbits as neutrons do here. In this heavier region, polarisation effects are reinforced as both types of nucleons share the same shape-driving character leading to strong cooperative effects. The parallels with the Cr isotopes are, indeed, quite striking. The odd-odd nuclei  $^{62}_{31}\text{Ga}_{31}$  and  $^{66}_{33}\text{As}_{33}$  [27,28] exhibit considerable softness with irregular low-lying levels, similar to the isotonic Cr systems, and, at higher excitation, fully-aligned  $[\pi g_{9/2} \otimes \nu g_{9/2}]_{J\pi=9^+}$  configurations are strongly populated. By  $^{70}_{35}\text{Br}_{35}$  [29], this configuration has fallen significantly in energy and appears as an oblate shape isomer whose only decay pathway is to non-yrast oblate states in  $^{70}\text{Se}$  [30], paralleling to some extent the structure of the  $9/2^+$  isomer in  $^{59}\text{Cr}$ . In heavier self-conjugate systems, the  $g_{9/2}$  occupancy increases to the extent that, even in the ground state, extremely deformed prolate shapes appear which are

associated with an  $N = 38$  gap. The detailed structure of the Cr isotopes close to  $N = 38$  is, therefore, of particular interest. The question arises whether the  $N = 40$  gap constrains Cr nuclei to near spherical, soft shapes or whether the  $\nu g_{9/2}$  occupancy is sufficient to generate well-deformed ground states.

In conclusion, systematic data for yrast  $9/2^+$  states in odd neutron-rich Cr nuclei suggest that the excitation of a  $g_{9/2}$  neutron is sufficient to polarise the soft core into a deformed shape. In  $^{55,57}\text{Cr}$ , low-lying negative-parity states appear to be roughly spherical in nature and the  $\nu g_{9/2}$  excitation produces a prolate shape and a decoupled rotational band based on the  $1/2^+[440]$  orbital. In  $^{59}\text{Cr}$ , a prolate shape is incompatible with the isomeric nature of the  $9/2^+$  state and it appears that the excitation of a  $g_{9/2}$  neutron drives an already mildly oblate core further towards oblate deformation. The development of polarisation across these isotopes has some parallels with the structure observed along the  $N = Z$  line.

## Acknowledgements

This work was supported by the UK Engineering and Physical Sciences Research Council, the US Department of Energy, Office of Nuclear Physics, under Contract Numbers W-31-109-ENG-38 and DE-FG02-94ER40848, and the US National Science Foundation under grant PHY-0139950. The authors would like to thank the group at Birmingham University for the use of their  $^{14}\text{C}$  target.

## References

- [1] M. Honma, T. Otsuka, B.A. Brown, T. Mizusaki, Phys. Rev. C 65 (2002) 061301.
- [2] J.I. Prisciandaro, et al., Phys. Lett. B 510 (2001) 17.
- [3] R.V.F. Janssens, et al., Phys. Lett. B 546 (2002) 55.
- [4] S.N. Liddick, et al., Phys. Rev. C 70 (2004) 064303.
- [5] B. Fornal, et al., Phys. Rev. C 70 (2004) 064304.
- [6] S.J. Freeman, et al., Phys. Rev. C 69 (2004) 064301; S.J. Freeman, et al., Phys. Rev. C 70 (2004) 029901, Erratum.
- [7] O. Sorlin, et al., Eur. Phys. J. A 16 (2003) 55.
- [8] S.J. Freeman, et al., AIP Conf. Proc. 764 (2005) 142.
- [9] S. Zhu, et al., in preparation.
- [10] P.F. Mantica, et al., Phys. Rev. C 67 (2003) 014311.
- [11] D.E. Appelbe, et al., Phys. Rev. C 67 (2003) 034309.
- [12] I.Y. Lee, Nucl. Phys. A 520 (1990) 641c.
- [13] C.N. Davids, et al., Nucl. Instrum. Methods B 70 (1992) 358.
- [14] A.M. Nathan, J.W. Olness, E.K. Warburton, J.B. McGrory, Phys. Rev. C 17 (1978) 1008.
- [15] D.E. Appelbe, et al., Eur. Phys. J. A 8 (2000) 153.
- [16] C.N. Davids, et al., Phys. Rev. C 17 (1978) 1815.
- [17] M. Honma, et al., Eur. Phys. J. A direct (2005) 10.1140/epjad/i2005-06-032-2.
- [18] M. Honma, private communication, 2005.
- [19] For example, R. Bock, et al., Nucl. Phys. 72 (1965) 273.
- [20] B.E. Chi, Nucl. Phys. 83 (1966) 97.
- [21] P.M. Endt, C. van der Leun, At. Data Nucl. Data Tables 13 (1974) 67.
- [22] F.R. Xu, P.M. Walker, J.A. Shiekh, R. Wyss, Phys. Lett. B 435 (1998) 257.
- [23] W. Nazarewicz, J. Dudek, R. Bengtsson, I. Ragnarsson, Nucl. Phys. A 435 (1985) 397.
- [24] R. Grzywacz, et al., Phys. Rev. Lett. 81 (1998) 766.
- [25] K. Langanke, et al., Phys. Rev. C 67 (2003) 044314.
- [26] J. Dudek, Z. Szymański, T. Werner, Phys. Rev. C 23 (1981) 920, and references therein.
- [27] D. Rudolph, et al., Phys. Rev. C 69 (2004) 034309.
- [28] R. Grzywacz, et al., Nucl. Phys. A 682 (2001) 41c.
- [29] D.G. Jenkins, et al., Phys. Rev. C 65 (2002) 064307.
- [30] M. Karny, et al., Phys. Rev. C 70 (2004) 014310.